Allosteric collaboration between elongation factor G and the ribosomal L1 stalk directs tRNA movements during translation

Jingyi Fei[a], Jonathan E. Bronson[a], Jake M. Hofman[b,1], Rathi L. Srinivas[c], Chris H. Wiggins[d], and Ruben L. Gonzalez, Jr.[a,2]

[a]Department of Chemistry, [b]Department of Physics, [c]The Fu Foundation School of Engineering and Applied Science, and [d]Department of Applied Physics and Applied Mathematics, Columbia University, New York, NY 10027

Communicated by Ignacio Tinoco, Jr., University of California, Berkeley, CA, July 22, 2009 (received for review May 22, 2009)

Determining the mechanism by which tRNAs rapidly and precisely transit through the ribosomal A, P, and E sites during translation remains a major goal in the study of protein synthesis. Here, we report the real-time dynamics of the L1 stalk, a structural element of the large ribosomal subunit that is implicated in directing tRNA movements during translation. Within pretranslocation ribosomal complexes, the L1 stalk exists in a dynamic equilibrium between open and closed conformations. Binding of elongation factor G (EF-G) shifts this equilibrium toward the closed conformation through one of at least two distinct kinetic mechanisms, where the identity of the P-site tRNA dictates the kinetic route that is taken. Within posttranslocation complexes, L1 stalk dynamics are dependent on the presence and identity of the E-site tRNA. Collectively, our data demonstrate that EF-G and the L1 stalk allosterically collaborate to direct tRNA translocation from the P to the E sites, and suggest a model for the release of E-site tRNA.

dynamics | single-molecule FRET | ribosome | translocation

During the elongation phase of protein synthesis, the ribosome repetitively cycles through three principal steps: (*i*) selection of an aminoacyl-transfer RNA (tRNA) at the ribosomal A site (1), (*ii*) peptidyl transfer from the P site-bound peptidyl-tRNA to the A site-bound aminoacyl-tRNA (2), and (*iii*) translocation of the messenger RNA (mRNA)-tRNA complex by one codon, effectively moving the P- and A-site tRNAs into the E- and P-sites, respectively (3). Perhaps the most dynamic steps of this cycle are the precisely directed mRNA and tRNA movements that occur during translocation (3–5). Although this step of the elongation cycle is promoted by elongation factor G (EF-G), numerous biochemical (6), structural (7, 8), and Förster resonance energy transfer (FRET) (9–15) studies have provided strong evidence that the peptidyl transfer step of the elongation cycle spontaneously triggers an EF-G-independent structural rearrangement of the ribosomal pretranslocation (PRE) complex that involves movements of the ribosome-bound tRNAs from their classical to their hybrid-bound configurations (6–10, 12), movement of the ribosomal L1 stalk from an open to a closed conformation (7, 8, 13, 15), and a counterclockwise, ratchet-like rotation of the small ribosomal subunit relative to the large subunit (7, 8, 11, 14).

Single-molecule FRET (smFRET) investigations have proven a powerful means for directly investigating the conformational dynamics of PRE complexes. Aided by X-ray and cryogenic electron microscopy (cryo-EM)-derived structural models, several groups have reported kinetic studies of tRNA and ribosome movements within PRE complexes (9, 10, 12–15). tRNA-tRNA smFRET ($smFRET_{tRNA\text{-}tRNA}$) experiments initially revealed that upon peptidyl transfer, tRNAs enter into a classical ⇄ hybrid dynamic equilibrium within PRE complexes (9, 10, 12). More recently, we have used an L1 stalk-tRNA smFRET ($smFRET_{L1\text{-}tRNA}$) signal to demonstrate that upon peptidyl transfer, a direct L1 stalk-tRNA contact is reversibly established (denoted as L1•tRNA) and disrupted (denoted as L1○tRNA), thus establishing an L1○tRNA ⇄ L1•tRNA dynamic equilibrium within PRE complexes. Using structural arguments, we proposed that L1○tRNA → L1•tRNA involved a classical → hybrid P-site tRNA transition as well as an open → closed L1 stalk transition and conversely, L1•tRNA → L1○tRNA involved a hybrid → classical P-site tRNA transition as well as a closed → open L1 stalk transition (13). Furthermore, kinetic analysis of the $smFRET_{tRNA\text{-}tRNA}$ and $smFRET_{L1\text{-}tRNA}$ signals suggested the possibility that, classical → hybrid and hybrid → classical P-site tRNA transitions might be directly coupled to open → closed and closed → open L1 stalk transitions, respectively, at least at our time resolution (0.05 sec frame^{-1}) (13). Unfortunately, at that time, the lack of a smFRET signal that could directly and independently report on the open and closed conformations of the L1 stalk precluded direct testing of these hypotheses.

Here, we describe a smFRET signal between ribosomal proteins L1 and L9 ($smFRET_{L1\text{-}L9}$) that reports directly on the open and closed conformations of the L1 stalk (Fig. 1). This $smFRET_{L1\text{-}L9}$ signal confirms that the L1 stalk indeed fluctuates between open and closed conformations within a PRE complex. Combined with our previous $smFRET_{tRNA\text{-}tRNA}$ and $smFRET_{L1\text{-}tRNA}$ studies, the data we present here provide strong support for a model in which L1○tRNA ⇄ L1•tRNA fluctuations are composed of coupled classical ⇄ hybrid P-site tRNA and open ⇄ closed L1 stalk transitions. Because the principal features of the PRE complex L1 stalk dynamics that we report here are in excellent agreement with those reported recently by Cornish et al. (15), we will primarily focus on those aspects of L1 stalk dynamics that have not been previously investigated. Specifically, we demonstrate that upon binding to PRE complexes, EF-G allosterically regulates the kinetics of L1 stalk fluctuations, employing one of at least two distinct kinetic strategies to shift the equilibrium toward the closed L1 stalk conformation; remarkably, the identity of the P-site tRNA dictates the kinetic strategy used by EF-G. In addition, we report L1 stalk dynamics in posttranslocation (POST) complexes and demonstrate that these depend on the presence and identity of the E-site tRNA. Based on our results, we propose a role for the L1 stalk in directing the release of deacylated tRNA from the E site.

Results

Single-cysteine variants of ribosomal proteins L1 and L9 were fluorescently labeled with Cy5- and Cy3-maleimides, respec-

Author contributions: J.F. and R.L.G. designed research; J.F. and R.L.S. performed research; J.E.B., J.M.H., and C.H.W. contributed new reagents/analytic tools; J.F. and J.E.B. analyzed data; and J.F. and R.L.G. wrote the paper.

The authors declare no conflict of interest.

[1]Present address: Yahoo! Research, 111 West 40th Street, 17th Floor, New York, NY 10018.

[2]To whom correspondence should be addressed. E-mail: rlg2118@columbia.edu.

This article contains supporting information online at www.pnas.org/cgi/content/full/0908077106/DCSupplemental.

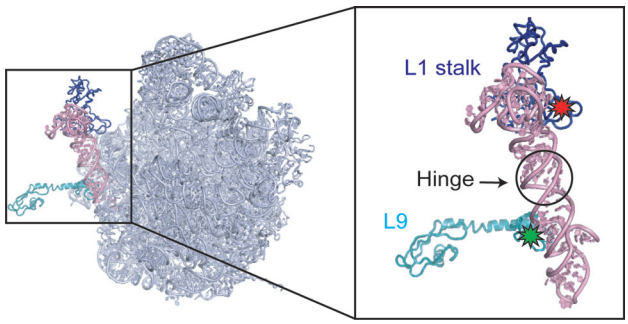

Fig. 1. Fluorescent labeling of ribosomal proteins L1 and L9 within the 50S ribosomal subunit. X-ray crystallographic structure of the 50S subunit (PDB ID code 2J01). The FRET donor (Cy3, green star) and acceptor (Cy5, red star) fluorophores are denoted at approximate positions on ribosomal protein L9 (cyan) and L1 (dark blue).

tively, and reconstituted into large, 50S ribosomal subunits purified from an L1/L9 double-deletion strain of *Escherichia coli* (Fig. 1). Functional testing of dual-labeled 50S subunits using a standard primer extension inhibition assay (16, 17) demonstrated ≈90% activity through the first round of translation elongation and ≈70% activity in a second round of translation elongation (*Methods*, supporting information (SI) *Methods* and Fig. S1).

Dual-labeled 50S subunits were used to enzymatically prepare a ribosomal initiation complex (INI) containing fMet-tRNA^{fMet} at the P site (9, 13, 18). Delivery of Phe-tRNA^{Phe}, in complex with elongation factor Tu (EF-Tu) and GTP in the presence of EF-G to INI generates a POST complex, POST$_{fM/F}$ (where the subscript denotes the presence of deacylated tRNA^{fMet} in the E site and fMet-Phe-tRNA^{Phe} in the P site) (9, 13, 18).

By using POST$_{fM/F}$ and INI, two PRE complexes were formed. Delivery of EF-Tu(GTP)Lys-tRNA^{Lys} to POST$_{fM/F}$ generates PRE$_{F/K}$ (where the F/K subscript now denotes deacylated tRNA^{Phe} at the P site and fMet-Phe-Lys-tRNA^{Lys} at the A site). Likewise, delivery of EF-Tu(GTP)Phe-tRNA^{Phe} to INI generates PRE$_{fM/F}$, carrying deacylated tRNA^{fMet} at the P site and fMet-Phe-tRNA^{Phe} at the A site (9, 13, 18). Two corresponding PRE-complex analogs were formed by reacting POST$_{fM/F}$ with puromycin to generate PMN$_{F/-}$, containing a deacylated tRNA^{Phe} at the P site and a vacant A site, and reacting INI with puromycin to generate PMN$_{fM/-}$, carrying a deacylated tRNA^{fMet} at the P site and a vacant A site (9, 13, 18) .

Analysis of steady-state smFRET vs. time trajectories reveals the presence of three trajectory subpopulations within each of the PRE/PMN complexes (Fig. 2). For all PRE/PMN complexes, the major subpopulation exhibits fluctuations between two well-defined FRET states centered at 0.56 ± 0.01 and 0.34 ± 0.01 FRET (Figs. 2 and 3). Based on close agreement with the smFRET$_{L1\text{-}L9}$ values predicted from cryo-EM reconstructions of the open and closed L1 stalk [≈0.67 FRET and ≈0.35 FRET, assuming R_0 ≈ 55 Å (19, 20)], the 0.56 and 0.34 FRET states were assigned to the open and closed L1 stalk conformations, respectively. Thus, we will refer to this trajectory subpopulation as SP$_{fluct}$. The remaining two subpopulations exhibit either stable 0.56 FRET (SP$_{open}$) or stable 0.34 FRET (SP$_{closed}$) before fluorophore photobleaching (Figs. 2 and 3). SP$_{open}$ is attributed to: (*i*) contaminating amounts of POST$_{fM/F}$ or INI that failed to react with EF-Tu(GTP)aminoacyl-tRNA or puromycin and (*ii*) PRE/PMN complexes that exhibited photobleaching directly out of the open conformation before undergoing a open → closed L1 stalk transition. SP$_{closed}$ is attributed to PRE/PMN complexes that exhibited photobleaching directly out of the closed conformation before undergoing a closed → open L1 stalk transition. We note here that PRE/PMN trajectories that occupy SP$_{open}$ and

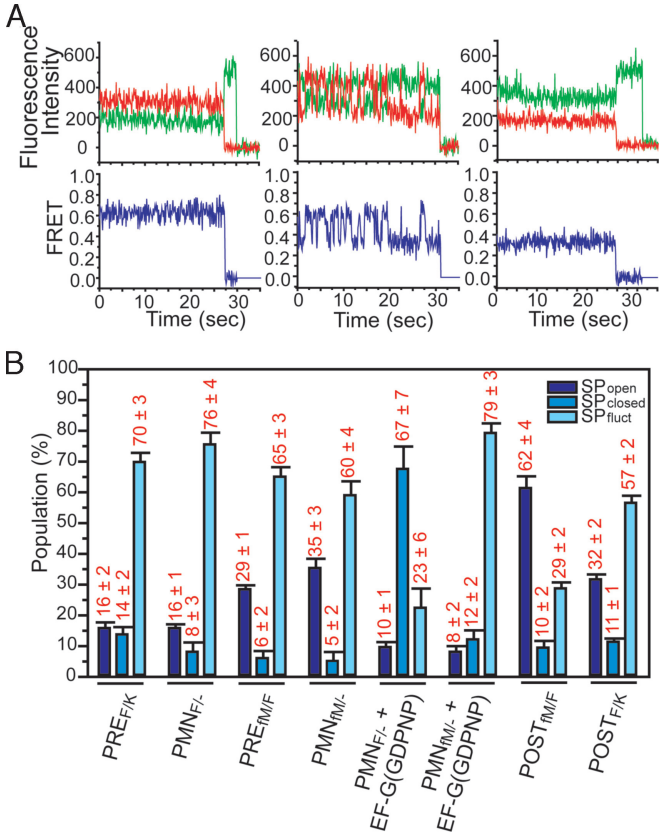

Fig. 2. Sample smFRET vs. time trajectories and relative occupancies of trajectory subpopulations. (*A*) Three subpopulations of trajectories were identified: stable 0.56 FRET (SP$_{open}$, *Left*), fluctuating between 0.56 and 0.34 FRET (SP$_{fluct}$, *Center*), and stable 0.34 FRET (SP$_{closed}$, *Right*). Representative Cy3 and Cy5 emission intensities are shown in green and red, respectively (*Upper*). The corresponding smFRET traces, $I_{Cy5}/(I_{Cy3}+I_{Cy5})$, are shown in blue (*Lower*). (*B*) The percentage of trajectories occupying SP$_{open}$, SP$_{fluct}$ and SP$_{closed}$ are shown as bar graphs for each complex. The mean and the standard deviation of the occupancy for each subpopulation in each complex, shown in red numbers, was calculated from four independent datasets.

SP$_{closed}$ do not correspond to static subpopulations of PRE/PMN complexes that are somehow distinct from the fluctuating subpopulation of PRE/PMN complexes. Rather, the occupancies of SP$_{fluct}$, SP$_{open}$, and SP$_{closed}$ are simply determined by a competition between open ⇄ closed L1 stalk transitions and photobleaching from the open and closed states (*Methods* and refs. 18 and 21; see also Table S1).

Fluctuations within SP$_{fluct}$ for all PRE/PMN complexes occur within one frame (Fig. 2), suggesting that open ⇄ closed L1 stalk transitions occur without sampling any intermediate state(s), at least not within our time resolution (0.10 sec frame^{-1}, see *SI Methods* for information regarding the time resolution of the smFRET data). Consistent with this, transition density plots reveal the existence of two major L1 stalk transitions, open → closed and closed → open, with no evidence of any significantly populated intermediate state(s) (Fig. S2).

Rates for L1 stalk closing and opening (k_{close} and k_{open}) were extracted by using dwell time analyses of SP$_{fluct}$ for all PRE/PMN complexes (*Methods*, Fig. S2, and Table 1). In addition, rates for the formation and disruption of the L1 stalk-tRNA contact ($k_{L1\bullet tRNA}$ and $k_{L1\circ tRNA}$) have been previously reported for PRE complexes analogous to PRE$_{F/K}$ and PMN$_{F/-}$ (ref. 13 and Table 1) and are measured and reported here for PRE$_{fM/F}$ and PMN$_{fM/-}$ (Fig. S3 and Table 1). Table 1 demonstrates the close agreement between k_{close} and $k_{L1\bullet tRNA}$ and between k_{open} and

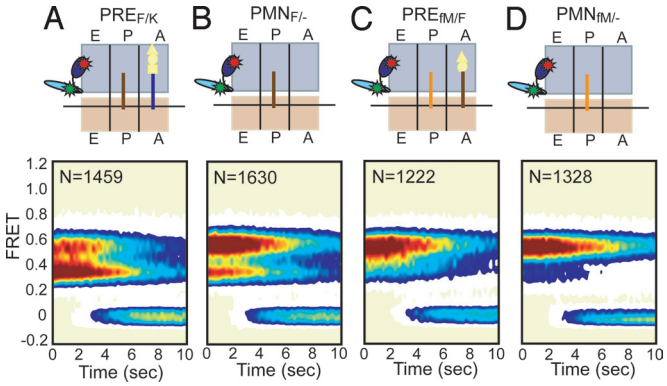

Fig. 3. The L1 stalk fluctuates between open and closed conformations in PRE/PMN complexes. Cartoon representations of the various complexes depict the 30S and 50S subunits in tan and lavender, respectively, with the L1 stalk in dark blue, L9 in cyan and tRNA^{fMet}, tRNA^{Phe}, and tRNA^{Lys} as orange, brown, and purple lines, respectively. Surface contour plots of the time evolution of population FRET are plotted from tan (lowest population) to red (highest population). The number of traces that were used to construct each surface contour plot is indicated by ''N.'' (*A*) PRE$_{F/K}$ was generated by addition of 100 nM EF-Tu(GTP)Lys-tRNA^{Lys} to POST$_{fM/F}$. (*B*) PMN$_{F/-}$ was generated by addition of 1 mM puromycin to POST$_{fM/F}$. (*C*) PRE$_{fM/F}$ was generated by addition of 100 nM EF-Tu(GTP)Phe-tRNA^{Phe} to INI. (*D*) PMN$_{fM/-}$ was generated by addition of 1 mM puromycin to INI.

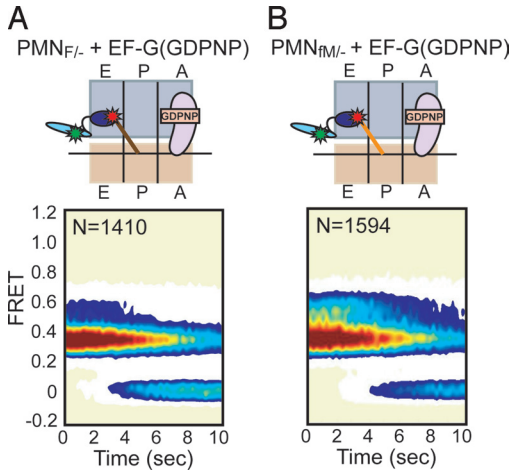

Fig. 4. EF-G allosterically regulates L1 stalk dynamics in a P-site tRNA dependent manner. Data are displayed as in Fig. 3. EF-G(GDPNP) (1 μM) was added to PMN$_{F/-}$ (*A*) and PMN$_{fM/-}$ (*B*).

$k_{L1\circ tRNA}$ for all PRE/PMN complexes. Significantly, k_{close} and k_{open} exhibit a dependence on the presence of an A-site peptidyl-tRNA that very closely mirrors the dependence observed for $k_{L1\bullet tRNA}$ and $k_{L1\circ tRNA}$ (compare changes in k_{close} to those in $k_{L1\bullet tRNA}$ and changes in k_{open} to those in $k_{L1\circ tRNA}$ for PRE$_{F/K}$ vs. PMN$_{F/-}$ and PRE$_{fM/F}$ vs. PMN$_{fM/-}$). The slight discrepancy between k_{close} and $k_{L1\bullet tRNA}$ in PRE$_{fM/F}$ vs. PMN$_{fM/-}$ most likely originates from the presence of the Cy3 fluorophore on tRNA^{fMet} in the $k_{L1\bullet tRNA}$ measurement (note that Cy3 on tRNA^{fMet} is at a different position than on tRNA^{Phe}) or, less likely, suggests that coupling between closing of the L1 stalk and movement of tRNA into the hybrid configuration might depend on the identity of P-site tRNA. Likewise, Table 1 demonstrates that k_{close} and k_{open} exhibit a dependence on the identity of the P-site tRNA that very closely mirrors the dependence observed for $k_{L1\bullet tRNA}$ and $k_{L1\circ tRNA}$ (compare changes in k_{close} to those in $k_{L1\bullet tRNA}$ and changes in k_{open} to those in $k_{L1\circ tRNA}$ for PRE$_{fM/F}$ vs. PRE$_{F/K}$ and PMN$_{fM/-}$ vs. PMN$_{F/-}$). Here, our observations are consistent with the well-documented propensity of tRNA^{fMet} to occupy the classical configuration (11, 22, 23). Collectively, our data provide strong support for the tight coupling of open $\rightarrow$ closed L1 stalk and classical $\rightarrow$ hybrid tRNA transitions on the one hand and closed $\rightarrow$ open L1 stalk and hybrid $\rightarrow$ classical tRNA transitions on the other.

We have previously shown that addition of 1 μM EF-G in the presence of GDPNP (a nonhydrolyzable GTP analog) to a PMN complex analogous to PMN$_{F/-}$ significantly inhibits L1$\bullet$tRNA $\rightarrow$ L1$\circ$tRNA transitions, thereby shifting the L1$\circ$tRNA $\rightleftarrows$ L1$\bullet$tRNA equilibrium strongly toward L1$\bullet$tRNA (13). In a completely analogous manner, addition of 1 μM EF-G(GDPNP) to PMN$_{F/-}$ strongly inhibits closed $\rightarrow$ open L1 stalk transitions such that the open $\rightleftarrows$ closed L1 stalk equilibrium shifts to favor the closed L1 stalk conformation, and the rate of photobleaching from the closed L1 stalk conformation effectively outcompetes closed $\rightarrow$ open transitions; the overall effect is a decrease in the occupancy of SP$_{fluct}$ and a corresponding increase in the occu-

Table 1. Transition rates for L1 stalk closing (k_{close}) and opening (k_{open}), as well as the formation ($k_{L1\bullet tRNA}$) and disruption ($k_{L1\circ tRNA}$) of the L1-tRNA interaction for PRE/PMN complexes

Complex	k_{close}, sec^{-1}	k_{open}, sec^{-1}	$k_{L1\bullet tRNA}$, sec^{-1}	$k_{L1\bullet tRNA}$, sec^{-1}
PRE$_{F/K}$	k_1 = 3.4 ± 0.4 (A_1 = 72 ± 8%) k_2 = 0.45 ± 0.12 (A_2 = 28 ± 8%)*	0.75 ± 0.14	k_1 = 2.9 ± 0.2 (A_1 = 70 ± 3%)† k_2 = 0.32 ± 0.05 (A_2 = 30 ± 3%)*†	0.85 ± 0.04†
PMN$_{F/-}$	0.51 ± 0.06	0.84 ± 0.17	0.43 ± 0.03†	1.06 ± 0.05†
PRE$_{fM/F}$	k_1 = 2.0 ± 0.6 (A_1 = 60 ± 2%) k_2 = 0.43 ± 0.06 (A_2 = 40 ± 3%)*	1.8 ± 0.3	k_1 = 2.8 ± 0.2 (A_1 = 73 ± 4%) k_2 = 0.69 ± 0.04 (A_2 = 27 ± 4%)*	3.0 ± 0.4
PMN$_{fM/-}$	0.37 ± 0.09	1.5 ± 0.3	0.36 ± 0.11	2.6 ± 0.2
PMN$_{F/-}$ + EF-G(GDPNP)‡	–	–	–	–
PMN$_{fM/-}$ + EF-G(GDPNP)	3.0 ± 0.6	1.2 ± 0.2	1.4 ± 0.1	1.54 ± 0.04

Rates reported here are the average and standard deviation from three or four independent datasets. All rates were corrected for photobleaching (see *Methods* and Table S1).

*The dwell time histograms for the open L1 stalk conformation and the disrupted L1 stalk-tRNA interaction in PRE$_{F/K}$ and PRE$_{fM/F}$ were better described by a double-exponential decay. The ≈30% population with the slower rate was assigned to complexes in which the peptidyl-tRNA has dissociated from the A site (9, 13, 38).

†Rates for the formation ($k_{L1\bullet tRNA}$) and disruption ($k_{L1\circ tRNA}$) of the L1-tRNA interaction in PRE$_{F/K}$ and PMN$_{F/-}$ were reanalyzed using vbFRET (see *Methods*) and the previously recorded raw data (13). Average values and standard deviations were calculated the as previously reported (13).

‡The major effect of EF-G(GDPNP) binding to PMN$_{F/-}$ is to shift the trajectory subpopulation occupancy towards SP$_{closed}$; thus, k_{open} and k_{close} for the EF-G(GDPNP)-bound fraction of PMN$_{F/-}$ cannot be calculated. Despite this, incomplete reactivity at each of the various enzymatic steps required to prepare PMN$_{F/-}$ yields a residual amount of partially-reacted complexes which result in trajectories that occupy SP$_{fluct}$ (see Fig. 2*B*). For details regarding this compositional heterogeneity of the PMN$_{F/-}$ sample and a detailed kinetic analysis of SP$_{fluct}$ for this sample, please see *SI Methods*, Fig S4, and Table S2.

pancy of SP_{closed} (Figs. 2 and 4A and Fig. S4). Because EF-G(GDPNP)-bound $PMN_{F/-}$ occupies SP_{closed}, k_{open}, and k_{close} for EF-G(GDPNP)-bound $PMN_{F/-}$ cannot be calculated (Table 1). Nevertheless, it is clear that without directly contacting either the P-site tRNA or the L1 stalk, binding of EF-G(GDPNP) to $PMN_{F/-}$ suppresses both L1•tRNA → L1○tRNA and closed → open L1 stalk transitions; this observation strongly suggests that during translocation, EF-G-ribosome interactions allosterically regulate tRNA as well as L1 stalk dynamics.

Addition of 1 μM EF-G(GDPNP) to $PMN_{fM/-}$ has a dramatically different effect than that observed for $PMN_{F/-}$. Rather than shifting the trajectory subpopulation occupancy toward SP_{closed}, binding of EF-G(GDPNP) to $PMN_{fM/-}$ leads to preferential occupancy of SP_{fluct} (Fig. 2 and Fig. S4). However, contour plots of the time evolution of population FRET reveal that, like $PMN_{F/-}$, $PMN_{fM/-}$ preferentially occupies the closed conformation of the L1 stalk in the presence of EF-G(GDPNP) (Fig. 4). To investigate the kinetic basis for the preferential occupancy of the closed L1 stalk conformation, we determined k_{close} and k_{open} for $PMN_{fM/-}$ in the absence and presence of 1 μM EF-G(GDPNP) (Table 1 and Table S2). The data in Table 1 demonstrate that EF-G(GDPNP) primarily increases k_{close} by ≈8-fold and has only a relatively minor effect on k_{open}. Thus, rather than suppressing closed → open L1 stalk transitions, as was observed for $PMN_{F/-}$, EF-G(GDPNP) increases k_{close} by destabilizing the open conformation of the L1 stalk in $PMN_{fM/-}$, resulting in an overall shift of the open ⇄ closed equilibrium analogous to what is observed for EF-G(GDPNP) binding to $PMN_{F/-}$ (i.e., the equilibrium shifts to favor the closed L1 stalk conformation). Here, the increased k_{close} and unchanged k_{open} yield a decrease in the occupancy of SP_{open} and a corresponding increase in the occupancy of SP_{fluct} and, to a lesser extent, SP_{closed} (Figs. 2 and 4). These results reveal that, although the overall effect of EF-G binding to PRE complexes is to shift the open ⇄ closed L1 stalk equilibrium toward the closed L1 stalk conformation, distinct kinetic mechanisms that depend on the identity of the P-site tRNA are used to accomplish this. Fully consistent with these results, $smFRET_{L1\text{-}tRNA}$ experiments on a PMN complex analogous to $PMN_{fM/-}$ reveal that in the presence of 1 μM EF-G(GDPNP), the majority of $smFRET_{L1\text{-}tRNA}$ trajectories fluctuate between L1○tRNA and L1•tRNA, with a preference for L1•tRNA that is primarily driven by an ≈4-fold increase in $k_{L1\bullet tRNA}$ (Fig. S3 and Table 1).

In addition to characterization of L1 stalk dynamics within PRE/PMN complexes, the $smFRET_{L1\text{-}L9}$ signal allows investigation of L1 stalk dynamics within POST complexes (Fig. 5). The majority of $POST_{fM/F}$ trajectories occupy SP_{open}, indicating a strong preference for the open L1 stalk conformation (Figs. 2 and 5*A*). Within SP_{fluct}, $k_{close} = 0.10 \pm 0.13\ sec^{-1}$ and $k_{open} = 0.99 \pm 0.16\ sec^{-1}$, also yielding a preference for occupying the open L1 stalk conformation. Because of heterogeneity in the tRNA occupancy of the E site, we generated a homogenous $POST_{-/F}$ complex by quantitatively dissociating $tRNA^{fMet}$ from $POST_{fM/F}$ (refs. 24 and 25 and Fig. S5). Fig. S6 shows that quantitative dissociation of the E-site tRNA decreases the occupancy of SP_{fluct} in favor of SP_{open}, strengthening the preference of the POST complex for the open L1 stalk conformation.

To test the generality of these results, we repeated these experiments on $POST_{F/K}$. In contrast to $POST_{fM/F}$, we find that only a minority of $POST_{F/K}$ trajectories occupy SP_{open}. Instead, the majority of $POST_{F/K}$ trajectories occupy SP_{fluct}, with $k_{close} = 0.31 \pm 0.09\ sec^{-1}$ and $k_{open} = 0.76 \pm 0.22\ sec^{-1}$, again generating a preference for the open L1 stalk conformation (Figs. 2 and 5*B*). Because heterogeneity in the E-site tRNA occupancy of $POST_{fM/F}$ and $POST_{F/K}$ is similar (Fig. S5), our data suggest that L1 stalk dynamics in POST complexes may depend on the identity of the E-site tRNA. Quantitative dissociation of deacylated $tRNA^{Phe}$ from the E site of $POST_{F/K}$ (Fig. S5) reveals that

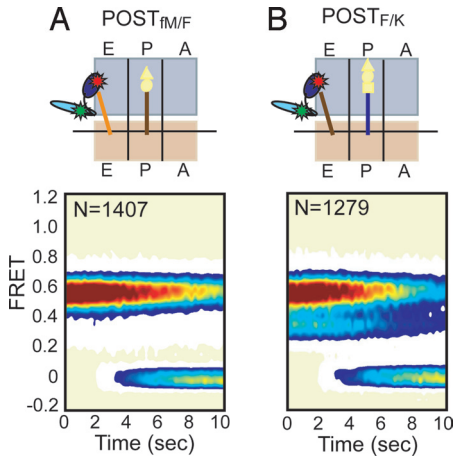

Fig. 5. The L1 stalk undergoes conformational dynamics within POST complexes. Data are displayed as in Fig. 3. (*A*) $POST_{fM/F}$. (*B*) $POST_{F/K}$ was generated by addition of 100 nM EF-Tu(GTP)Lys-$tRNA^{Lys}$ and 1 μM EF-G(GTP) to $POST_{fM/F}$.

the majority of $POST_{-/K}$ trajectories occupy SP_{open}, completely analogous to our observations on $POST_{-/F}$ (Fig. S6). Thus, although the L1 stalk within POST complexes exhibits an overall preference for the open conformation, the kinetics underlying this preference depend on the presence and identity of the E-site tRNA. This observation implies that each tRNA species might make slightly different and unique binding interactions with the ribosomal E site.

To assess the dynamics of the L1 stalk within a homogeneous POST complex containing a fully occupied E site, we artificially delivered 1 μM deacylated $tRNA^{fMet}$ to $POST_{-/F}$ to generate $POST_{fM^*/F}$ and deacylated $tRNA^{Phe}$ to $POST_{-/K}$ to generate $POST_{F^*/K}$. In stark contrast to our results for $POST_{fM/F}$ and $POST_{F/K}$, containing authentically translocated E-site tRNAs, we find that the majority of $POST_{fM^*/F}$ and $POST_{F^*/K}$ trajectories preferentially occupy the closed L1 stalk conformation (compare Fig. 5*A* with Fig. S6*D* and Fig. 5*B* with Fig. S6*E*). Preliminary subpopulation and kinetic analysis of $POST_{fM^*/F}$ and $POST_{F^*/K}$ (Fig. S6) indicate that, similar to our results for POST complexes containing authentically translocated E-site tRNAs, L1 stalk dynamics in POST complexes containing artificially delivered E-site tRNAs may also depend on the identity of the E-site tRNA. It should be stated, however, that possible compositional heterogeneity arising from the incomplete binding of deacylated tRNA to the ribosomal E site and/or from reverse translocation of $POST_{fM^*/F}$ and $POST_{F^*/K}$ (these experiments were conducted in the absence of EF-G) (26, 27) precludes detailed subpopulation and kinetic analysis. Regardless, it is clear that although authentically translocated E-site tRNAs exhibit a strong preference for the open conformation of the L1 stalk, artificially delivered E-site tRNAs instead generate a preference for the closed L1 stalk conformation. Presumably, this closed L1 stalk conformation is identical to the "half-closed" conformation that has been observed by Cornish et al. in similarly prepared POST complexes (i.e., containing an artificially delivered E-site tRNA) (15). Thus, it seems that our $smFRET_{L1\text{-}L9}$ signal cannot distinguish between the fully closed L1 stalk conformation observed in PRE/PMN complexes and the half-closed L1 stalk conformation observed in POST complexes containing an artificially delivered E-site tRNA; this is perhaps not surprising given the smaller dynamic range of the $smFRET_{L1\text{-}L9}$ signal in this work relative to the L1-L33 smFRET signal in Cornish et al. (15) Thus, whether or not the half-closed L1 stalk conformation observed by Cornish et al. in POST complexes containing artificially delivered E-site tRNAs is sampled in POST complexes contain-

ing authentically translocated E-site tRNAs remains to be determined. Regardless, our results demonstrate that L1 stalk dynamics within POST complexes are sensitive to the mechanism through which the deacylated tRNA enters the E site.

Discussion

Previously, we have proposed that PRE/PMN complexes spontaneously and reversibly fluctuate between two major conformational states: global state 1 (GS1), encompassing classically bound tRNAs, an open L1 stalk and a nonratcheted ribosome and global state 2 (GS2), encompassing hybrid-bound tRNAs, a closed L1 stalk and a ratcheted ribosome (13). Consistent with this model, our $smFRET_{L1\text{-}L9}$ results demonstrate that the L1 stalk within PRE/PMN complexes exists in an open ⇄ closed dynamic equilibrium that exhibits kinetics closely matching those of the classical ⇄ hybrid tRNA (9) and the L1∘tRNA ⇄ L1•tRNA (13) dynamic equilibria. Most notably, all three equilibria have matching kinetic responses toward the occupancy of the A site by a peptidyl-tRNA and the identity of the P-site tRNA. These kinetic data demonstrate the close coupling between tRNA and L1 stalk dynamics within PRE/PMN complexes. In addition to our $smFRET_{tRNA\text{-}tRNA}$ (9), $smFRET_{L1\text{-}tRNA}$ (13) and $smFRET_{L1\text{-}L9}$ studies, further support for the GS1 ⇄ GS2 model is provided by two recent smFRET studies from Ha, Noller, and coworkers demonstrating the close correlation between the equilibrium constants governing the nonratcheted ⇄ ratcheted ribosome and open ⇄ closed L1 stalk equilibria (14, 15). In complete agreement with the smFRET results and the GS1 ⇄ GS2 model, two recent cryo-EM studies applied particle classification methods to reveal the existence of two major PRE complex conformations within a single pretranslocation sample, corresponding to GS1 and GS2, respectively (7, 8). Despite the excellent agreement between the GS1 ⇄ GS2 model and the available smFRET and cryo-EM data, however, it remains possible that short-lived and/or rarely sampled intermediates within GS1 → GS2 and/or GS2 → GS1 transitions have thus far eluded detection by smFRET experiments or cryo-EM reconstructions. Future smFRET experiments recorded at higher-time resolution or using ribosome-targeting small-molecule translocation inhibitors or mutagenized ribosomes may prove useful tools for uncovering such short-lived and/or rarely sampled intermediates. Nevertheless, the GS1 ⇄ GS2 model represents a simple dynamic model that is consistent with the available data and provides a convenient framework for describing the global dynamics of the translating ribosome.

Binding of EF-G(GDPNP) to PMN complexes strongly shifts the open ⇄ closed L1 stalk equilibrium toward the closed conformation by regulating k_{open} and/or k_{closed}. Given that EF-G(GDPNP) binds near the A site of the PRE complex, ≈170 Å away from the hinge region of the L1 stalk (28–31), our data demonstrate that EF-G(GDPNP) regulates L1 stalk dynamics allosterically, through its interactions with the ribosome upon binding to the PMN complex. An attractive hypothesis, consistent with the close coupling of ratcheting, L1 stalk and tRNA dynamics stipulated by the GS1 ⇄ GS2 model, is that EF-G(GDPNP) establishes interactions with the ribosome that directly stabilize the ratcheted conformation of the ribosome, indirectly leading to stabilization of the hybrid P-site tRNA configuration and the closed L1 stalk conformation. Indeed, the discovery that vacant *Saccharomyces cerevisiae* ribosomes (i.e., not containing tRNA substrates) predominantly exist in a ratcheted conformation with a closed L1 stalk (32) suggests the possibility that the coupling between intersubunit ratcheting and L1 stalk closure might be independent of the presence of a P-site tRNA and may instead be encoded within the architecture of the ribosome itself. Evidence for a similar possibility in prokaryotic ribosomes comes from the correlation between the equilibrium constants governing the nonratcheted ⇄ ratcheted ribosome and open ⇄ closed L1 stalk equilibria in vacant *E. coli* ribosomes (14, 15); the correlation between the forward and reverse rates of these two processes, however, remains to be investigated. Regardless, in this framework, ratcheting and L1 stalk closure would function allosterically to promote and stabilize the hybrid tRNA configuration during translocation. Future experiments exploring the role of ribosomal structural elements in regulating ratcheting, L1 stalk and tRNA dynamics should allow testing of these hypotheses.

Using $smFRET_{L1\text{-}tRNA}$ and $smFRET_{L1\text{-}L9}$ signals as reporters for the GS1 ⇄ GS2 equilibrium, we find that EF-G(GDPNP) can shift the GS1⇄ GS2 equilibrium toward GS2 through at least two distinct kinetic mechanisms, the choice of which is regulated by the identity of the P-site tRNA. When $tRNA^{Phe}$ occupies the P site, EF-G(GDPNP) almost completely suppresses GS2 → GS1 transitions whereas when $tRNA^{fMet}$ occupies the P site, EF-G(GDPNP) has an almost negligible effect on GS2 → GS1 transitions, instead increasing the rate of GS1 → GS2 transitions by ≈4- to 8-fold. This latter result strongly suggests that EF-G can bind directly to PRE complexes in the GS1 state and actively promote the GS1 → GS2 transition, although the extent to which this is observed strongly depends on the identity of the P-site tRNA.

The conformational dynamics of the L1 stalk observed within POST complexes, which are likely uncoupled from intersubunit ratcheting dynamics because POST complexes are not expected to ratchet (11, 14, 30), are altogether distinct from those observed within PRE/PMN complexes. We find that L1 stalk dynamics within POST complexes are sensitive to the presence and identity of the E-site tRNA as well as to the mechanism through which the tRNA enters the E site. In the presence of a vacant E site, the L1 stalk is almost uniformly found in the stable open conformation. The presence of an authentically translocated E-site tRNA, however, triggers open ⇄ closed L1 stalk fluctuations where k_{open} and k_{close} depend on the identity of the E-site tRNA. Despite the differing kinetics, POST complexes containing either authentically translocated $tRNA^{fMet}$ or $tRNA^{Phe}$ both favor the open L1 stalk conformation; this stands in contrast with the uniformly half-closed L1 stalk conformation observed within POST complexes containing an artificially delivered E-site tRNA (15) and in X-ray crystal structures of POST-like ribosomes carrying what are likely artificially delivered E-site tRNAs (33–35). Consistent with these observations, we find that artificial delivery of a deacylated tRNA into the E site of a POST complex triggers a strong preference for the closed L1 stalk conformation.

Previously we have reported a stable (i.e., nonfluctuating) high FRET signal between the L1 stalk and an authentically translocated E-site tRNA within a POST complex (13). In contrast, the data we present here demonstrates that the L1 stalk within an analogous POST complex, under identical sample conditions as our previous study, undergoes open ⇄ closed fluctuations. To reconcile these two observations, we propose a model in which the authentically translocated E-site tRNA is reconfigured within the E site such that the direct interaction between the tRNA and the L1 stalk is maintained during the open ⇄ closed fluctuations of the L1 stalk. This model is strongly supported by the observation that the E-site tRNA occupies one configuration in X-ray crystal structures of POST-like complexes bearing a closed, or half-closed, L1 stalk conformation (33–35) but occupies a notably different E-site tRNA configuration in cryo-EM reconstructions of POST complexes bearing an open L1 stalk conformation (30). As originally suggested by the authors of the cryo-EM study (30), reconfiguration of the E-site tRNA such that a direct contact with the opening L1 stalk is maintained may be mechanistically important for E-site tRNA release. That said, we find that k_{open} is ≈10-fold faster than the rate of passive tRNA dissociation from the E site in POST

complexes, indicating that the L1 stalk/E-site tRNA can undergo numerous fluctuations before the E-site tRNA dissociates and strongly suggesting that opening of the L1 stalk is not rate limiting for E-site tRNA release. Finally, the observation that L1 stalk dynamics within a POST complex depend on the identity of the E-site tRNA may reflect a difference in the energetics of reconfiguring each tRNA species within the E site. The molecular basis for this difference likely originates from the slightly different interactions that each tRNA would be expected to make with structural elements of the ribosomal E site.

Collectively, our data demonstrate that differences in the interactions of $tRNA^{fMet}$ and $tRNA^{Phe}$ with the elongating ribosome can: (*i*) bias the kinetics of GS1 ⇄ GS2 transitions in PRE/PMN complexes; (*ii*) control the kinetic mechanism through which EF-G stabilizes the GS2 state during translocation; and (*iii*) regulate tRNA and L1 stalk dynamics within POST complexes. It remains to be investigated whether these differences are due to tRNA identity elements that uniquely distinguish initiator $tRNA^{fMet}$ from all elongator tRNAs (36), thus suggesting that elongator tRNAs will generally exhibit kinetic behavior similar to $tRNA^{Phe}$, or whether similarly significant differences in kinetic behavior will be found even among elongator tRNAs. Future smFRET studies using an expanded set of elongator tRNAs and/or $tRNA^{fMet}$ variants containing mutations to $tRNA^{fMet}$ identity elements, should reveal which features of tRNA structure and tRNA-ribosome interactions are involved in regulating the kinetic behavior of PRE/PMN and POST complexes.

Methods

All experiments were performed in Tris-polymix buffer (50 mM Tris-OAc, 100 mM KCl, 5 mM NH_4OAc, 0.5 mM $Ca(OAc)_2$, 10 mM 2-mercaptoethanol, 5 mM putrescine and 1 mM spermidine) at 15 mM $Mg(OAc)_2$ and at $pH_{25\,°C} = 7.5$ (9). smFRET trajectories were recorded by using a home-built total internal reflection fluorescence microscope (13, 18). Each smFRET trajectory was idealized as a hidden Markov model, by using the vbFRET software package (37). Dwell times spent in each state before transitioning were extracted from the idealized smFRET trajectories and the lifetime of each state was determined by exponential fitting of the corresponding one-dimensional population vs. time histogram (9, 13, 18). Transition rates were calculated by taking the inverse of the lifetimes and correcting for the rate of photobleaching from each state. Full methods and references can be found in the *SI Methods*.

ACKNOWLEDGMENTS. We thank S. Das for managing the R.L.G. laboratory; J. Frank, H. Gao, and X. Agirrezabala for providing us with GS1 and GS2 structural models; and M. M. Elvekrog, D. D. MacDougall, and S. H. Sternberg for valuable discussions and comments on the manuscript. This work was supported by Burroughs Wellcome Fund Grant CABS 1004856 (to R.L.G.), National Science Foundation (NSF) Grant MCB 0644262 (to R.L.G.), National Institutes of Health (NIH)–National Institute of General Medical Sciences Grant 1RO1GM084288-01 (to R.L.G.), NIH Grants 1U54CA121852-01A1 and 5PN2EY016586-03 (to C.H.W.), and an NSF Research Experience for Undergraduates grant (to R.L.S.).

1. Daviter T, Gromadski KB, Rodnina MV (2006) The ribosome's response to codon–anticodon mismatches. *Biochimie* 88:1001–1011.
2. Beringer M, Rodnina MV (2007) The ribosomal peptidyl transferase. *Mol Cell* 26:311–321.
3. Shoji S, Walker SE, Fredrick K (2009) Ribosomal translocation: One step closer to the molecular mechanism. *ACS Chem Biol* 4:93–107.
4. Frank J, et al. (2007) The process of mRNA-tRNA translocation. *Proc Natl Acad Sci USA* 104:19671–19678.
5. Moran SJ, et al. (2008) The mechanics of translocation: A molecular ''spring-and-ratchet'' system. *Structure (London)* 16:664–672.
6. Moazed D, Noller HF (1989) Intermediate states in the movement of transfer RNA in the ribosome. *Nature* 342:142–148.
7. Agirrezabala X, et al. (2008) Visualization of the hybrid state of tRNA binding promoted by spontaneous ratcheting of the ribosome. *Mol Cell* 32:190–197.
8. Julian P, et al. (2008) Structure of ratcheted ribosomes with tRNAs in hybrid states. *Proc Natl Acad Sci USA* 105:16924–16927.
9. Blanchard SC, et al. (2004) tRNA dynamics on the ribosome during translation. *Proc Natl Acad Sci USA* 101:12893–12898.
10. Kim HD, Puglisi JD, Chu S (2007) Fluctuations of transfer RNAs between classical and hybrid states. *Biophys J* 93:3575–3582.
11. Ermolenko DN, et al. (2007) Observation of intersubunit movement of the ribosome in solution using FRET. *J Mol Biol* 370:530–540.
12. Munro JB, Altman RB, O'Connor N, Blanchard SC (2007) Identification of two distinct hybrid state intermediates on the ribosome. *Mol Cell* 25:505–517.
13. Fei J, Kosuri P, MacDougall DD, Gonzalez RL, Jr (2008) Coupling of ribosomal L1 stalk and tRNA dynamics during translation elongation. *Mol Cell* 30:348–359.
14. Cornish PV, Ermolenko DN, Noller HF, Ha T (2008) Spontaneous intersubunit rotation in single ribosomes. *Mol Cell* 30:578–588.
15. Cornish PV, et al. (2009) Following movement of the L1 stalk between three functional states in single ribosomes. *Proc Natl Acad Sci USA* 106:2571–2576.
16. Hartz D, McPheeters DS, Traut R, Gold L (1988) Extension inhibition analysis of translation initiation complexes. *Methods Enzymol* 164:419–425.
17. Fredrick K, Noller HF (2002) Accurate translocation of mRNA by the ribosome requires a peptidyl group or its analog on the tRNA moving into the 30S P site. *Mol Cell* 9:1125–1131.
18. Sternberg SH, et al. Translation factors direct intrinsic ribosome dynamics during termination and ribosome recycling. *Nat Struct Mol Biol* 16:861–868.
19. Bastiaens PI, Jovin TM (1996) Microspectroscopic imaging tracks the intracellular processing of a signal transduction protein: Fluorescent-labeled protein kinase C beta I. *Proc Natl Acad Sci USA* 93:8407–8412.
20. Hohng S, Joo C, Ha T (2004) Single-molecule three-color FRET. *Biophys J* 87:1328–1337.
21. Bartley LE, et al. (2003) Exploration of the transition state for tertiary structure formation between an RNA helix and a large structured RNA. *J Mol Biol* 328:1011–1026.
22. Dorner S, Brunelle JL, Sharma D, Green R (2006) The hybrid state of tRNA binding is an authentic translation elongation intermediate. *Nat Struct Mol Biol* 13:234–241.
23. Studer SM, Feinberg JS, Joseph S (2003) Rapid kinetic analysis of EF-G-dependent mRNA translocation in the ribosome. *J Mol Biol* 327:369–381.
24. Nierhaus KH (1990) The allosteric three-site model for the ribosomal elongation cycle: Features and future. *Biochemistry* 29:4997–5008.
25. Semenkov YP, Rodnina MV, Wintermeyer W (1996) The ''allosteric three-site model'' of elongation cannot be confirmed in a well-defined ribosome system from *Escherichia coli*. *Proc Natl Acad Sci USA* 93:12183–12188.
26. Shoji S, Walker SE, Fredrick K (2006) Reverse translocation of tRNA in the ribosome. *Mol Cell* 24:931–942.
27. Konevega AL, et al. (2007) Spontaneous reverse movement of mRNA-bound tRNA through the ribosome. *Nat Struct Mol Biol* 14:318–324.
28. Wilson KS, Noller HF (1998) Mapping the position of translational elongation factor EF-G in the ribosome by directed hydroxyl radical probing. *Cell* 92:131–139.
29. Agrawal RK, Penczek P, Grassucci RA, Frank J (1998) Visualization of elongation factor G on the *Escherichia coli* 70S ribosome: The mechanism of translocation. *Proc Natl Acad Sci USA* 95:6134–6138.
30. Valle M, et al. (2003) Locking and unlocking of ribosomal motions. *Cell* 114:123–134.
31. Connell SR, et al. (2007) Structural basis for interaction of the ribosome with the switch regions of GTP-bound elongation factors. *Mol Cell* 25:751–764.
32. Spahn CM, et al. (2004) Domain movements of elongation factor eEF2 and the eukaryotic 80S ribosome facilitate tRNA translocation. *EMBO J* 23:1008–1019.
33. Yusupov MM, et al. (2001) Crystal structure of the ribosome at 5.5 A resolution. *Science* 292:883–896.
34. Korostelev A, Trakhanov S, Laurberg M, Noller HF (2006) Crystal structure of a 70S ribosome-tRNA complex reveals functional interactions and rearrangements. *Cell* 126:1065–1077.
35. Selmer M, et al. (2006) Structure of the 70S ribosome complexed with mRNA and tRNA. *Science* 313:1935–1942.
36. Varshney U, Lee CP, RajBhandary UL (1993) From elongator tRNA to initiator tRNA. *Proc Natl Acad Sci USA* 90:2305–2309.
37. Bronson JE, Fei J, Hofman JM, Gonzalez RL, Jr, Wiggins CH (2009) Learning rates and states from biophysical time series: A Bayesian approach to model selection and single-molecule FRET data. arXiv:0907.3156 [q-bio.QM], http://arxiv.org/pdf/0907.3156.
38. Semenkov YP, Rodnina MV, Wintermeyer W (2000) Energetic contribution of tRNA hybrid state formation to translocation catalysis on the ribosome. *Nat Struct Biol* 7:1027–1031.